A. A. ElFouly / ICEHM2000, Cairo University, Egypt, September, 2000, page 293- 310

# Faults and Fractures Intersections Delineation as a Tool for Groundwater Detection Using Remote Sensing and Ground Penetrating Radar Techniques at Saint Catherine area, Southern Sinai, Egypt.

***Adel Elfouly***
*Geology Department, and Center for Environmental Hazards Mitigation,*
*Cairo University, Giza, Egypt*
*Tel./Fax.#: (202)5540593*
*Email: AdelElFouly@OREX.ORG*

**Abstract:** This study demonstrates an optimal use of the extracted lineaments from Landsat-5 images for ground water detection at Saint Catherine area. The comparison between the use of lineaments density (LD) and density of lineaments intersection (DLI) is discussed showing why the density of lineaments intersection (DLI) is more efficient in this type of research. The structural analysis and interpretation of the DLI is deeply discussed, verifying the structural relation between the main faults trends and the proposed water conduits in the system. The delineation of the most favorate locations for the underground water aquifer depends mainly on the areas that have the highest watershed and the highest density fractures intersection. Ground penetration radar technique has successfully been used to confirm ground water detection in the area according to the proposed model.

**Key Words:**
Lineaments intersection, fracture analysis, fluid flow, watershed, GPR, ground penetrating radar, Reidel shear

## Introduction:

In recent years, remote-sensing methods have been increasingly recognized as a means of obtaining crucial geoscientific data for both regional and site-specific investigations. Remote-sensing data provides a synoptic perspective not achievable with traditional field studies. The methods applied in this study are effective for basic and applied research covering ground water detection. Remote-sensing methods are recommended in this study because they can provide geoscientific data for large areas in relatively short time. Whenever possible, remote-sensing data should be acquired and integrated into the early stages of an investigation and used in conjunction with traditional mapping techniques.

Studies of ground-water flow through fractured rock have focused on the physical characteristics of the fractures including aperture, spacing, length, and connectivity (long and Witherspoon, 1985; Domenico and Schwartz, 1990; Sharp, 1993; and National Research Council, 1996) and the local fracture pattern (Thorpr, 1980; de Marsily, 1985; Collins et al., Frieldman and Wiltschko, 1992; Fuller and Sharp, 1992; Laubach, 1992). One old approach to obtaining the local fracture pattern is by scanline mapping of fractures exposed in outcrops. Scanline mapping is a procedure whereby a geologist records the attitude and physical characteristics for all discontinuities that intersect a horizontal or vertical line that parallels the outcrop surface. La Pointe and Hundson (1985) discuss some of the drawbacks to scanline mapping and ways to improve the results. In this study, lineaments have been extracted directly from digital TM Landsat-5 image after a series of enhancements and bands ratioing.
The widely used lineaments density has been compared with the density of lineaments intersection that has been adapted in this study. The watershed modeling is applied and the ground penetrating radar measurements are used to confirm water detection in the proposed location at Saint Catherine area.

## Geology

The study area (about 1332.5 km2) is bounded by latitudes 28°25’52.2” and 28°48’ 35.12” N and longitudes 33°51’13.68”and 34°09’58.34” E (Fig.1). It includes the highest

mountainous peaks in Sinai (2637m + MSL at G. Catherine). The area receives an annual precipitation of about 62mm, which is higher than surrounding areas of South Sinai. Precipitation occurs mostly during the periods from October to December and from March to May. A maximum monthly precipitation of 76.2mm was recorded during November 1937. Frequently, the area is subjected to flash floods after heavy showers that precipitate in short duration. The air temperature varies between 23° and 32°C during summer and between 9° and 12° C during winter. The temperature drops below zero about twenty times a year. The high peaks are hence covered with a thin snow layer.

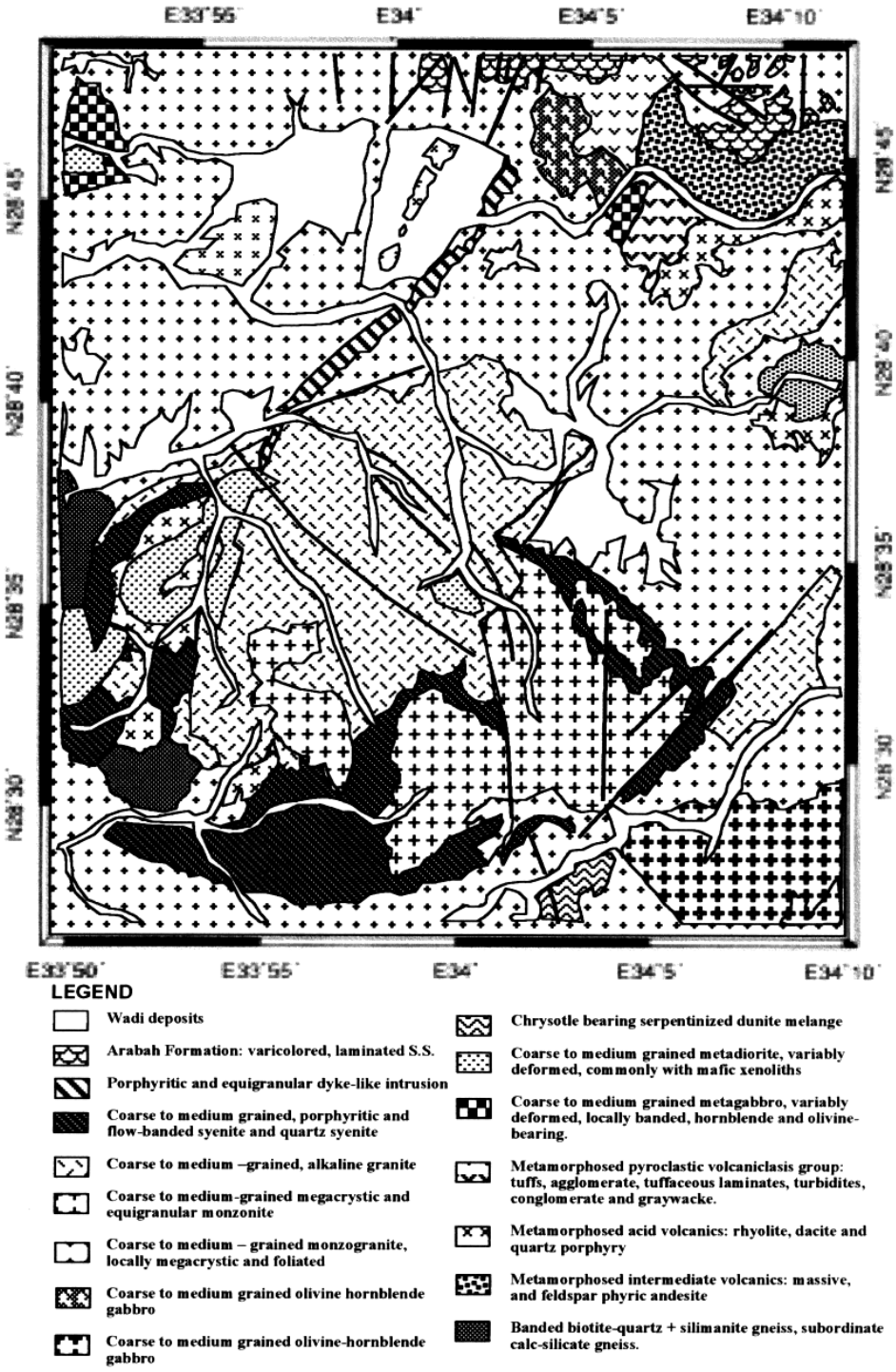


Fig.1 Geologic map of Saint Catherine area, from the Geological map of Sinai, Sheet NO.1, 1994. Geologic survey of Egypt, Arab Republic of Egyt.

The regional hydrogeologic setting is Sinai basement province was studied by several workers; e.g. El-Ghawaby and Kassem (1982), Issar and Gland (1982), El-Shazly et al. (1985), El-Shamy et al (1989), Shendi (1989) and El-Rayes (1992). Exploration for more water resources is an important task for developing St. Catherine area to face the growing touristic demands of that area.

St. Catherine area is covered by medium and coarse-grained granites, granodioritic-dioritic association, monzonites, syenites, Catherine volcanics and Rutig volcanics (El – Rayes, 1992). These rocks are dissected by dykes. The diorites, granodiorites and monzonites form low to medium hills with gentle slopes. In contrast granites, with the overlying thick volcanic sheets, form high mountains with extended flat-topped plateaus and steep slopes.

Drainage is controlled by large-scale fracture systems. The different rock units are highly affected by several faults and joints with different trends and densities. The most dominant fault trends are N-S, NE-SW, NW-SE and NNW-SSE. Some less dominant trends are represented by ENE-WSW and NNE-SSW. Such structures govern a widely distributed hydrographic system.

Less resistant basic dikes tend to form elongated depressions. The permeability of alluvial fill in the wadis varies greatly from place to place, ranging from impermeable to permeable, where it forms major aquifer, e.g., at the confluence of several wadis or in major alluvial fans.

The wadis alluvial fill consists of gravel to boulder size rocks mixed with fine clastics. The alluvial cover vary in thickness 30 and 100m and are composed of the existing wadis is greater at the upstream parts whereas the downstream parts show moderate to low gradients.

## Procedure of study:

In this study, TM Landsat-5 image enhancement and processing for lineament analysis has been accomplished. The comparison between the lineaments density and density of lineaments intersection and their role in lineament analysis are discussed. Watershed delineation and area selection for GPR measurements will be accomplished in the following procedures.

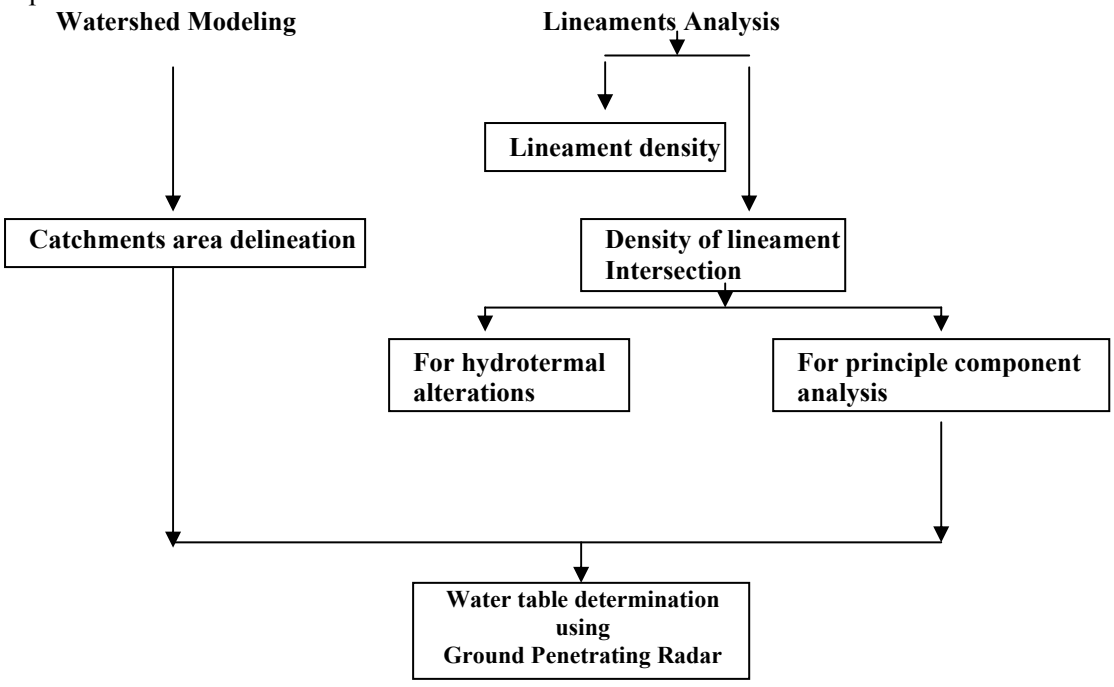


### A) Watershed Delineation

A watershed is described as the total area of water flowing to a given outlet point or more often known as pour point. The boundary between two adjacent watersheds is the drainage line. Pour point is the point at which the water flows out of the area.

This is the lowest point in elevation along the boundary or the drainage lines. Delineation of watersheds depends on the catchment drainage pattern of the watershed (Fig. 5). This in turn depends on the relief of the area considered. While considering the digital representation of the terrain using the degital elevation model (DEM), errors in data, such as artificial minimum points can lead to large numbers of watersheds, which needs to be overcome by suitable preprocessing the data. The steps involved in delineation of watershed including preprocessing of the digital elevation data are discussed in the following paragraphs. The preprocessing step includes remodal of artificial depressions (sinks) by an interative process. Superimposition of existing drainage in DEM if necessary, generation of flow direction from each cell, calculation of flow accumulation by accumulating the weight for all cells that flow into each down slope cell and derivation of watershed is carried out by interactively selecting an outfow point on the stream network. The size of the watersheds generated is controlled by the number of cells that need to flow into a cell to classify it as a stream. Watersheds of different sizes can be achieved by giving different threshold values while building the stream network ( Fig. 5 and 6). The watershed boundaries definition for Saint Catherine area is delineated as shown in figure 6.

**B) Lineament analysis:**

The Density of lineaments intersection method is implied in this study. This method relay mainly on the detection of the fractures associated with faults (ElFouly, 2000). Many pinnate or feather fractures that are arrayed en-echelon along shear fracture form as extension fractures during shearing and they are oriented approximately perpendicular to the minimum compressive stress when they form (fig. 2c & 2d ) some pinnate fractures may also originate as secondary shear fractures such as the R Riedel shears (fig. 2c, 2d and 2e) or P secondary shears. The acute angles between the fault and both the extension fractures and the R Riedel shears point in the direction of relative motion of the fault block containing the secondary shear fractures.

The delineation of areas of high favorability for groundwater detection is defined as the main objective in this study. They are considered the areas of high underground water potentiality that demonstrate the characteristics of having water catchment area and provide the highest density of lineament intersection.

## B1- Data Preparation for lineament analysis:

Data preparation and TM Landsat-5 image bands selection are designed to reach the objective of this study. The principle component analysis and multispectral band ratioing will be discussed in the following paragraphs.

- Principal component Transformation:

Principal component (also called by the names Hotelling, discrete Karhunen-Loeve, or eigenvector) transformation is an image enhancement technique for displaying the maximum spectral contrast from n spectral bands with just three primary display colors, and it involves a two-step process that is briefly described here (A more complete description of principal component transformations is given in Hall 1979). The first step inputs n histograms of the image, one histogram per spectral band, to the principal component algorithm. This algorithm calculates n principal components, which are actually orthogonal vectors in n-dimensional space that are oriented along directions of maximum remaining variance. Outputs of this first step are the projection coefficients of the n spectral bands onto the final n principal components, yielding the series of equations given below:

$$P_k = \sum_{i=1}^{n} a_{i,k}\, DN(i)$$

where $P_k$ is the $k^{th}$ princial component value for a given pixel, DN(i) is the digital number of the $i^{th}$ spectral band (out of a total of n spectral bands) for a given pixel, and $a_{i,k}$ are the

projection coefficients calculated by the principal component algorithm for projecting digital numbers from the n spectral bands onto the n principal component vectors.

The first principal component is a vector that is in the direction of the maximum variance of pixels in the scene. It accounts for more of the spectral variance in the data than any other principal component. The first principal component is usually dominated by illumination effects arising from differences in slope aspect relative to the sun and provides a good noise-free representation of topography. Spectral reflectance features of surface materials and noise appear in higher-numbered PCs (e.g., Mouat et al., 1986; Amos and Greenbaum, 1987; Eriksen and Cowan, 1989; Frei and Jutz, 1989; Rodrigeuz and Glass, 1991; Bennett, 1993).

Principle components analysis is applied to 6 subset of the 7 TM Landsat-5 channels data sets( bands 1,2,3,4,5 and 7). The number of components produced is equal to six channels analyzed. The Largest percentage of the total scene variance is included in the first component (PC1) as shown in figure 3a.

- Multispectral band ratioing

Spectral ratioing is a multispectral image processing method that involves the division of one spectral band by another, usually after some preliminary corrections have been made for atmospheric path radiance and/or additive offset introduced by the multispectral sensor. The spectral bands employed for a spectral ratio image (the image manifestation of a spectral ratio) are usually selected such that one spectral band is inside and the other is outside a wavelength region of spectral reflectance minimum or maximum of a particular target. Spectral ratios are attractive because they enhance compositional information, while suppressing other types of information about Earth's surface, such as terrain slope and grain size differences.

The interband ratioing of multispectral images enhances subtle spectral reflectance or color differences between surface materials that are often difficult to detect in standard images. Ratioing accentuates color differences while removing first order brightness or albedo variations caused by totography (Lyon 1977). The analysis of Crippen (1988) and experience of numerous investigators have shown TM 5/7 discriminate materials containing hydroxyl-bearing minerals. These minerals can be used as good indicator for the water effects along fractures.

## B2- Lineament density and Density of Lineaments Intersections calculation and comparison:

In the following the operators used to extract the lineaments and their intersections will be provided, and comparative study for the commonly used lineament density calculation and the newly developed density of lineaments intersection procedures.

- Lineament classifier:

El-Fouly, 1992 and El-Fouly et.al., 1992, introduced a highly non-linear logic operators to extract lineaments and their intersections from Landsat-5 images and involve simple arithmetic differences between adjacent pixels for gradient calculation, followed by a series of table lookups and logical binary decisions to determine the presence or absence of the feature of interest. The operator performs a series of computations in the selected direction(s) up to four orientations. If a feature of interest is found, a pixel is marked. To extract the lineament intersections instead of using the logic OR as shown in the valley and ridge operator (Fig 2a&2b), the logic AND will simply detect the lineaments intersection in the selected directions. In this study, the two diagonal and two axial directions have been used.

At figures 3b and 4b we can observe how lineament can be detected in different ways to serve different objectives. In figure 3b we can concider it as the actual lineaments in the area because it was extracted from the first principle component (PC1) but in figure 3c the lineaments are extracted from the enhanced image for hydrothermal alterations, In this case, we are extracting only lineaments related to these alterations. As we can observe in the

comparison between figure 3b and 4b, that presence and the distribution of the lineaments are generally different.

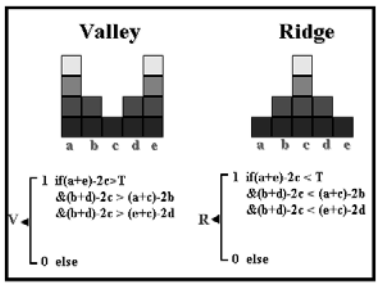


Figure 2a, Lineament classification using logic operator.
(Reproduced after ElFouly, 2000)

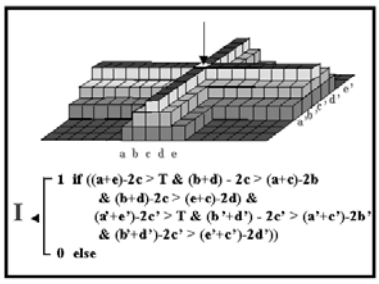


Figure 2b, Lineament intersection logic operator along 2- axial directions.
(Reproduced after ElFouly, 2000)

- The Lineaments density (LD)

The lineaments density is counting the number of lineaments extracted by the lineament classifier in figure 3b and 4b per kilometer square. The density of lineaments presented areas and the numbers are reflected by the intensity distribution and strength as shown in figure 3c and 4c. In figure 3c, the highest numbers of extracted lineaments are mainly related to the granitoid alkaline granitic intrusion and the phorphyritic dyke like intrusion in the south western and central part of the study area taking a NE-SW trend. Figure 4c, the highest intensity of lineaments are strongly related to the caldera struture in the southeastern part and concentrated in the northwestern part of Saint Catherine area.

-The Density of lineaments intersection

The densities of lineament intersection analysis and its application can be described using the faulting produced in the experiments carried out by Wilcox, Harding and Seely (1973). These experiments exemplifies the geometry and kinematics of Riedel shearing, which is characteristic of, but not limited to, strike-slip faulting. The synthetic strike-slip faults are Riedel shears (R-shears), and they form at an acute angle about 15° to the main line of faulting (Figure 2c). Their arrangement is en echelon, which means that they are parallel to one another and arranged along a common line of bearing. The antithetic strike-slip faults are conjugate Reidel shear (R'-shears), and they form at a high angle of about 75 ° to the main line of faulting (Figure 2c). The direction of greatest principal stress ($\sigma_1$) bisects the angle between R and R'. As strike-slip faulting along the main zone proceeds, R-shears achieve a closer angle with the main line of faulting, and R'-shears may be rotated to higher angle. Furthermore, a new set of synthetic shears may be rotated to a higher angle. Furthermore, a new set of synthetic shears known as P-shears develop, and these form at a small acute angle 10° to the main line of faulting (Figure 2c). The arrangement of R-shears, R'-shears, and P-shears is that as "minor" faults they can together be used to independently interpret the sense of movement for the main line of faulting as a whole through their points of intersections. Additionally, the whole concept of Riedel shearing gives us a better sense of why strike-slip fault zones have a braided appearance and how the points of intersections will help us delineate the main line of faulting. (Figure 2d). By calculating the density of the intersected minor faults, and interpolating the output, the density of lineaments intersections map will be produced the elongated pattern in this map can point a main line of faulting in the area.

The density of lineaments intersection is produced by counting the number of lineaments intersections per kilometer square.The DLI will help delineate main shear zones. Main fracture systems can be clearly delineated as show in the black and white dashed lines in figure 3d and 4d. The DLI related to the enhanced hydrothermaly altered lithology in the area

can be observed in figure 4d. The high intensities are generally restricted in southern half of the map associated with the porphyritic, banded and quartz syenites and their related rocks. This alteration occupies the caldera structure of Saint Catherine and generally shows high relief. In the north eastern corner most of the alterations are located at the north eastern part of the NW-SE fault system and mainly restricted at moderate relief areas.

Since DLI related to the calculated first principle component of the study area which have the largest percentage of the total scene variance, represent the intensity and location of the possible conduits related to most lithologic unit in the area. The high values of the normalized density of lineament intersection values per kilometer square around the porphyritic dyke like intrusion in the eastern part of the area and trending NNE-SSW, in the monzogranite alkali granite in the western and central part of the area and in the olivine hornblende granite in the southeastern corner of saint catherine area.

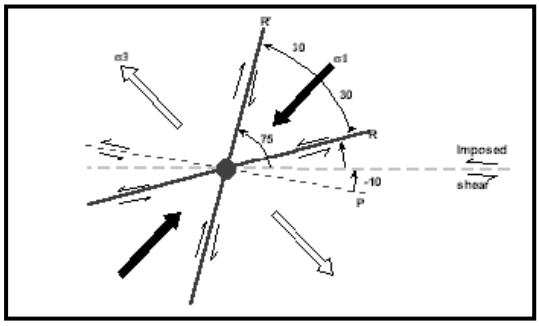


Figure 2c, In the left-handed strike slip zone. Riedel shear arrays for both left handed faulting. R and R' are conjugate Riedel shears; R is synthetic, whereas R' is antithetic to the main movement. R and R' form first. P shears come is a little later.
(Modified after Woodcockand Schubert (1994))
Lineaments Intersection

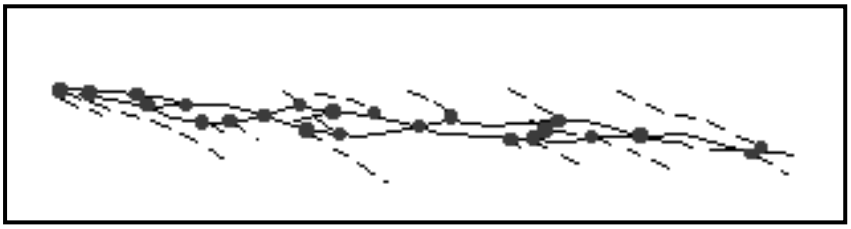

Figure 2d, In this right-handed strike-slip zone the interrelationships of Riedel shears, splays, and P shears combine to produce a braided shear pattern. (Modified after Woodcockand Schubert (1994))
Lineaments Intersection

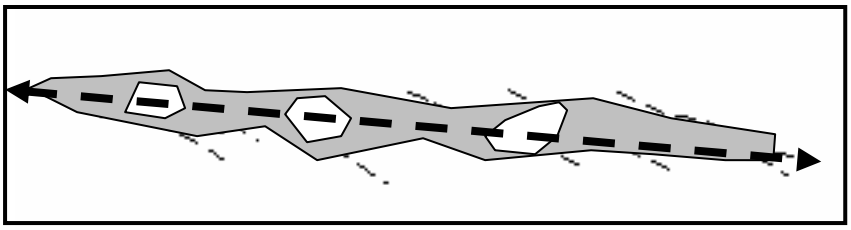

Figure 2e, Calculated density of lineament intersection extracted in figure 2d, representing an elongated pattern to delineate the main line of faulting.

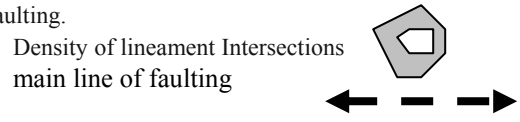

- Area delineation for Ground water determination:

As mentioned before the objective of this study is to delineate areas of high favorability for groundwater detection. That is accomplished by calculating the water catchment area,(fig. 6 ) and demonstrating the highest density of lineament intersection (DLI) (fig. 7).

The DLI for the hydrothermal alteration enhanced image cannot serve our goal in this study because it shows strong relation with high temperature hydrothermal activity, but it could be very valuable form mineral exploration. The DLI for the first principle component (PC1) will be used in this study for conduit delineation in the various rock units in the area. Thresholding for 25% of the high intensity values of the normalized density of lineaments intersection per kilometers square, have been applied for the DLI of the first principle component (PC1) (Fig. 3d) to produce a binary map for the areas of the highest density of lineament intersection in Saint Catherine area as shown in figure 7. The distributions of these intensities are dominated along the eastern and western side of the study area.

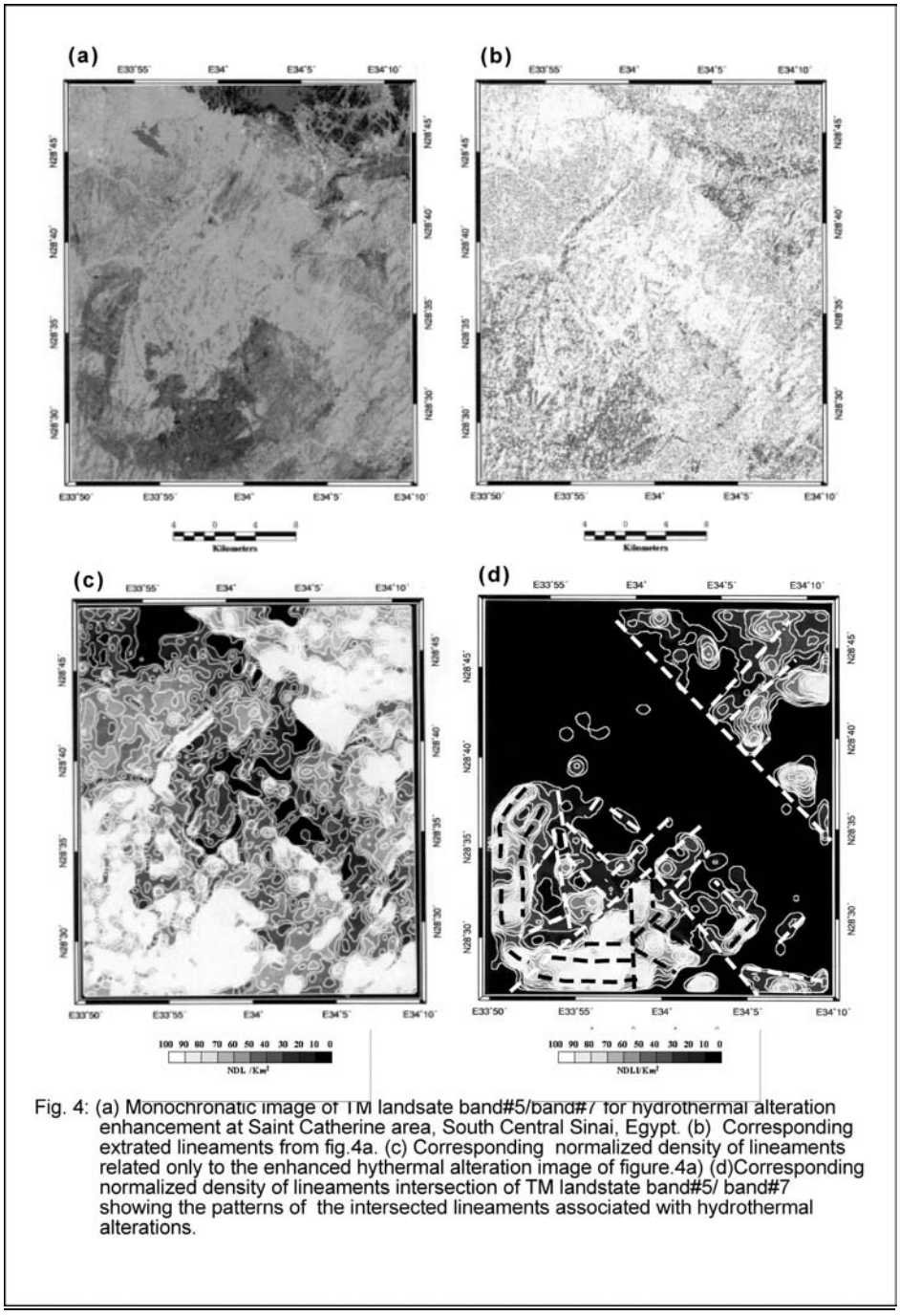


Fig. 4: (a) Monochronatic image of TM landsate band#5/band#7 for hydrothermal alteration enhancement at Saint Catherine area, South Central Sinai, Egypt. (b) Corresponding extrated lineaments from fig.4a. (c) Corresponding normalized density of lineaments related only to the enhanced hythermal alteration image of figure.4a) (d)Corresponding normalized density of lineaments intersection of TM landstate band#5/ band#7 showing the patterns of the intersected lineaments associated with hydrothermal alterations.

Figure 6, shows the catchment areas that demonstrate the highest DLI. That is accomplished by overlying by using the "IDRISI" geographic information system by Clark University, U.S.A. The white color, in figure 8, represents the catchments area that has the highest density of lineaments intersection in the study area. Location (a) and (b) in figure 8 are selected places for ground penetrating radar (GPR) measurements for ground water detection.

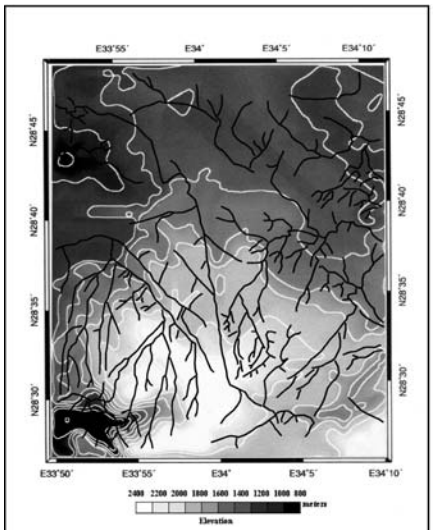

Fig. 5. The drainage patterns of Saint Catherine area super imposed of its Digital Elevation Model .

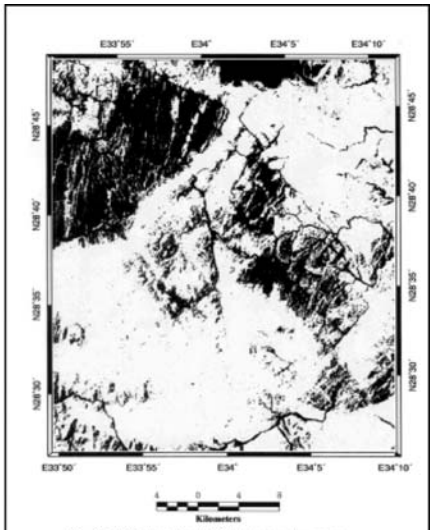

Fig. 6. Watershed Catchment areas at Saint Catherine area, South Central Sinai, Egypt.

Catchment areas

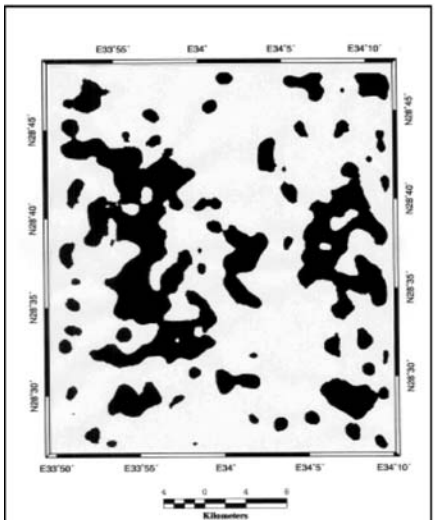

Fig. 7. Threshoded density of lineaments intersection the first princlple component of figure 3d.

Areas of high density of lineament intersection

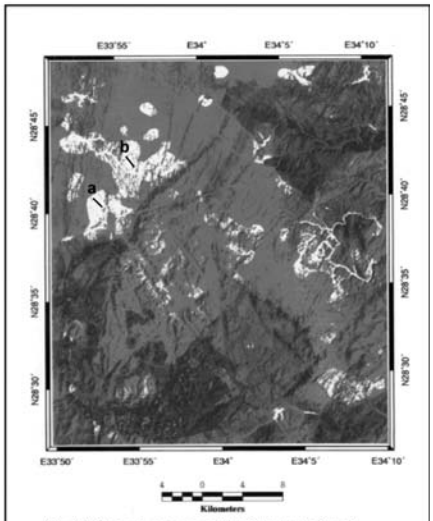

Fig. 8 Shows areas with high density of lineament intersection that occur in watershed Catchment areas and overlained in white color on band5/7 of at Saint Catherine area TM image

GPR survey line

## C) Water table determination using Ground Penetrating Radar

Introduction

Ground Penetrating Radar (GPR) is a geotechnical surveying technique that uses electromagnetic energy in the form of a high-frequency pulse generated from a transmitting antenna (Moorman el.al., 1994). The apparatus typically consists of "antenna skis", which can be interchanged depending upon frequency desired, fiber optic cables connecting the skis to a personal field computer, and a power source. The radiated wavefront travels down into the

earth, encountering differences in electrical properties that are associated with the various subsurface lithologies.

The propagation and characteristics of the electromagnetic wave are characterized mathematically by Maxwell's equations. When the wavefront hits a boundary, some of the energy is reflected back to the surface. At the surface, a receiver antenna records the reflected energy. This receiver records the time it takes for the pulse to travel down to the reflector and back to the surface. The travel time of the wavefront is a function of the type of lithology through which the energy travels as well as distance down to the reflector.

Ground Penetrating Radar frequency is related to depth of penetration and resolution of the survey. Lower frequency tends to have deep penetration and low resolution, while the higher frequencies have shallow penetration and high resolution (Fetter, 1994).

There are many factors that may affect quality of GPR data. Terrain electrical conductivity of the site plays an important role in determining the depth of penetration of the radar pulse (Robillard el al., 1994). For consolidated rocks, depth of penetration has a maximum of around 100 feet (shale-limestone or sandstone with no soil cover). It has been shown that in areas of high conductivity, such as clay-rich soil, the depth penetration can be minimal. On the other hand, depth of penetration generally reaches a maximum at sites, which consist of little or no clay. Reflector depth can be determined from velocity of the electromagnetic wave and reflection time as recorded at the surface. Attenuation of the energy in various lithologies also limits depth of penetration. This is a result of energy being lost from "spherical spreading and exponential material losses with contributions from conversion of electromagnetic energy to thermal energy through electrical conduction losses, dielectric relaxation losses in water, or diffusion-limited chemical diffusion in clay minerals" (Beres, 1991).

A variety of man-made features are not very common in Saint Catherine area, which may disturb or influence GPR surveys. Some of the features are power lines, large trees and metallic objects.

Two ground penetrating radar (GPR) data sets were acquired at location (a) and (b) at the north western part of the study area. (See locations in figure 9). The goal of the surveys is to image the fluvial cobble and sand stratigraphy. The data sets were acquired using 25 MHz antennas. Depth of penetration reach up to ~ 60 m. Processing significantly improves the reliablity and vertically into several distinct units or radar architectural elements.

-Data Acquisition

We used a RAMAC GPR system from Mala Geosiences, Inc., for all data acquisition. The antennas had center frequencies of 25 MHz. All of the data were acquired using the common-offset reflection profiling method. The transmitter-receiver separation for the 25 MHz data is 4 m.The survey length measures ~ 40 m along the valley. Station spacing along each line is 0.5 m.

- Processing:

The data is processed, using GRADIX software from Interpex limited, to improve image quality. The first step in processing was to input geometry information and edit headers. Next, a short (3-sample) temporal median trim filter was applied to each trace to attenuate noise spikes that contaminated some of the data. A background dc level was present in all of the data sets. The dc level was removed by calculating the average amplitude before the first breaks and removing this value from each sample of each trace. A residual median filter was then applied to attenuate the wow. Test show that this filter successfully attenuates both the low and high-frequency components of wow, without adding precursors or other artifacts to the wavelets. (Gerlitz et al., 1993). Time zero determination and ldatuming was also performed.

The next step in the processing sequence was amplitude compensation. For each line, we determined the rectified-amplitude versus time fall-off of the data. The inverse of this curve was scaled by a multiplier (0.3) to form the gain function. The multiplier is used to reduce the gain function somewhat so that anomalously high amplitude values are not clipped after

amplitude compensation. The direct air and ground waves were attenuated by subtracting the average trace for each line from each trace. The net effect is that the air wave is almost completely removed. After the static corrections, the water table can be seen as a horizontal surface in the uppermost part of each line (Fig. ). Finally, a bandpass filter (20~300 MHz) and an AGC function is applied for dispay.

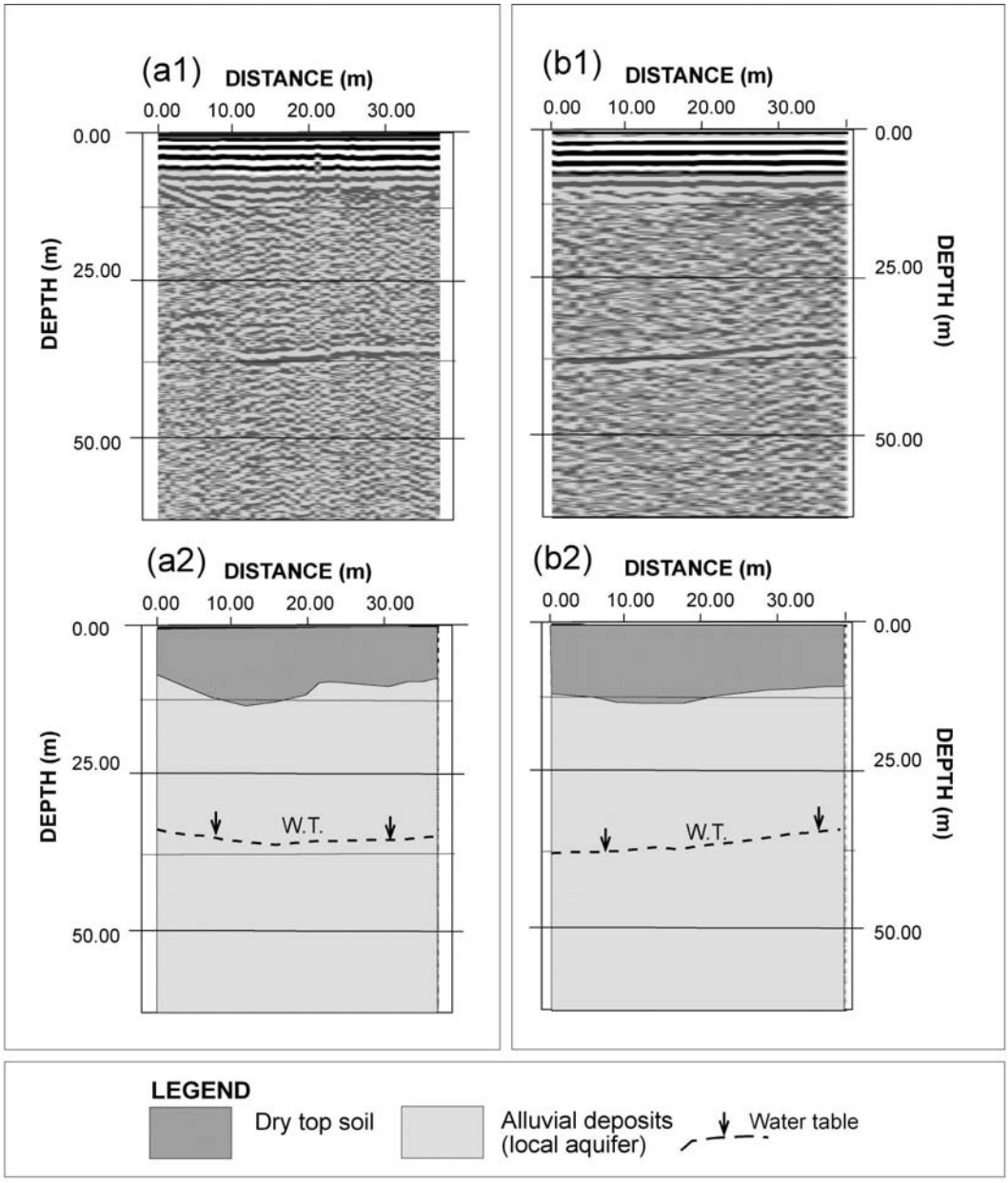


Fig. 9. Interpretation of two 35 meters length GPR reflection profiles at St. Catherine area (see location a and b at figure 8). Water table can be detected arround 35 meters depth.

- Water table determination

The determination of the water table has been an ongoing topic of discussion between practitioners of GPR. Our research has shown that GPR is extremely sensitive to the detection of the water table depends upon the host material, which establishes the z capillary fringe in the vadose zone. As shown in Figure 9a& 9b, it is indicated that the effective water table for GPR reflections was actually the capillary fringe in this area. It is clear that strong water table reflections only occur in very clean (clay-free) sand and rock.

Water table monitoring is strongly recommended for different seasons in the Saint Catherine area. Changes in water table depth can be monitored using GPR. Water table arises from increase in water content in soil. Repeat GPR survey at time intervals to detect changes in water table level.

## Discussion :

Lineaments, in representing fundamental zones of weakness in the lithosphere, offer such high permeability pathways via dilational zones, and may continue to provide them over long periods of geological time. Lineaments analysis has provided useful information in fracture permeability aquifers. One must be aware of the possibility that the important fracture directions in the aquifer may not be the same as those most readily apparent at the surface (Prost,1988). These may happen because the aquifer was fractured in a stress regime that had ended before deposition of the rocks at the surface. Fracture studies can also be useful in understanding the nature of an aquifer that may already be producing from fractures. The fractures may be permeability pathways or even, in some cases, permeability barriers. Surface fracture mapping can help plan and evaluate secondary recovery programs where there is a likelihood of fractures controlling the flow of subsurface fluids (Prost, 1996). Fracture can behave as impermeable barriers to flow by preventing the movement of aquifer fluids across the fracture zone and by channeling the fluids along the zone parallel to the trend of the fractures.

The mapping of linear features associated with fractures (faults and joints) can be performed from images of almost any wavelength region. This type of mapping is an important ground water exploration tool for metamorphic and igneous terrain, because the greatest amount of water will be found near fractures, where the only porosity and permeability will be located. One of the assumptions made in the past about igneous and metamorphic terrain is that the greatest amounts of water could be found where the greatest fracture length density (total line miles of fractures per square mile) occurs (Vincent et al. 1978). However, that early reasoning has proved to be somewhat simplistic, in that later evidence has shown that some fractures are more productive of ground water than others, and in some metamorphic terrain, folds can be as important as fractures.

The major structure in Saint Catherine area caused by tensional fractures due to the collapse structure of the oval shaped Caldera occupying the central and southern part of the study area. Li (1994) recently found that in granitic rocks, fractures that were caused by tensional forces often contained more water than compressional fractures. The reason given by Li (1994) for this was that tensional fractures are wider than compressional fractures. However, tensional forces often cause en echelon fractures (sets of parallel fractures). This process provides yet another reason for more ground water to be found along tensional fractures. Invoking a single porosity model, this assumes that almost all flow is along fractures and not in the igneous and metamorphic bedrock.

Ramasamy and Jayakumar (1993) have shown that in complexity folded and fractured Precambrian rocks of the Southern Indian peninsula, some aquifer systems were controlled by total linear density and total linear intersection density, some were controlled by linear intersections and release fractures (thin, tight fractures parallel to the fold axes and restricted mostly to the axial portion of the anticlines and synclines), and some were controlled by extension and shear fractures.

Ground-water flow in fractured-rock aquifer is controlled by the aperture, length, filling, roughness, spacing and connectivity of the fractures that make up the fracture network along with the local state of stress (Gale, 1982; Gale et al., 1985; Long and Witherspoon, 1985; Nelson, 1985; Domenico and Swartz, 1990; and Sharp, 1993). In this study, the density of lineament intersection procedure is used to focus on the connectivity of the identified fracture sets is each domain.

The DLI related to the enhanced hydrothermal alteration in the area (Fig. 4d). The high intensities are generally restricted in collapsed caldera struture of Saint Catherine. The DLI for the hydrothermal alteration inhanced image cannot serve our goal in this study because it shows strong relation with high temperation hydrothermal activity, could be very valuable form mineral exploration and the caliche in these fractures indicates that surface water has and may still be infiltrating these fractures, but since these fractures have a lower potential for connectivity, it is less likely that water can migrates through these fracture systems.

Faults can be conduits that allows fluid flow or barriers that block fluid flow or a combination of both where sections are barriers and others are conduits. Several conditions can cause a fault to be barriers to fluid flow, including juxtaposition of strata with high hydraulic conductivity against strata with high hydraulic conductivity and the development of gouge that has a hydraulic conductivity less than the surrounding rock (Smith, 1966).

## Summary:

In this study, lineaments analysis has been used for groundwater detection by using the remote sensing and geographic information systems techniques. The Ground Penetrating Radar Technique is used to delineate the watertable at Saint Catherine area, Southern Sinai, Egypt.

For data preparation, the TM Landsat-5 image enhancement and processing for lineament analysis has been accomplished by using the principal component analysis and the multispectral band ratioing. The first component of the principal component analysis is selected for the density of lineaments intersections extraction due its posation of the largest percentage of the total scene variance. That will guarantee the presence of most of the lineaments associated with all the geologic and structural components of the study area.The multispectral band ratioing for TM Landsat-5 image for band 5/7 is prepared before the extration of the density of lineaments intersections (DLI) to enhance the hydrothermally altered lithology in the area. That will help in the extraction of the DLI that are only related to hydrothermal activities.

This technique was expected to help in tracing the surface water path through the fracture systems in the area, but unfortunatly it shows the high tempreture hydrothermal and sussessfuly traced the collapse structures of the Saint Catherine Caldera in the area. The comparison between the use of lineaments density (LD) and density of lineaments intersection (DLI) is discussed showing why the density of lineaments intersection (DLI) is more efficient in this type of research. The DLI help delineate major structure system in the area and point sussessfully to conduits suitable for fluid path ways in the study area.

The lineament classifier (ElFouly, 1994) is used to extracte lineaments and their intersections to calculate lineament density (LD) and the density of lineaments intersections. The lineaments densities reflect the intensity and distribution of the lineaments (Fig.3c and 4c) and the density of lineaments intersections show the intensity and the distribution of the intersected lineaments. That inturn will help delineate the major shear zones in the area (Fig. 3d and 4d).

The steps involved in the delineation of watershed including preprocessing of the digital elevation data of the study area to generate the flow direction and calculate the flow accumulation that flow into each down slope and the derivation of watershed is carries out by interactively selecting an outflow point on the stream network. The watershed boundaries are delineated as shown in figure 6.

The ground penetrating radar technique is used for water table determination. In this study we used a RAMAC GPR system from Mala Geosiences, Inc., for all data acquisition. The antennas had center frequencies of 25 MHz. The data is processed using GRADIX software from Interpex limited. It is indicated that the effective water table for GPR reflections was actually the capillary fringe in this area (Fig. 9).

## Conclusion:

In this research the following have been accomplished:

1- The comparison of two different approaches for:
   a- data preparation toward lineament extraction (1st principle component vs. TM image ratioing of band 5/7)
   b- for lineaments density calculations (the lineaments density and the density of lineaments intersections)

2- The delineation of areas with high favorable underground water potentiality by integrating water catchment areas with areas of high density of lineament intersection.

3- Underground water detection is accomplished successfully by using the Ground penetrating radar technique by showing satisfatory results for watertable detection and results is confirm with nearby local wells.

This study demonstrates the optimal use of the lineaments that have been extracted from TM Landsat-5 images for ground water detection at Saint Catherine area. The efficiency of DLI for this type of research is discussed through the comparison between the use of lineaments density (LD) and density of lineaments intersection (DLI). The LD demonstrates good capability for extension and intensity delineation of fractures in the study area. The LD outputs will not serve effectively our objectives in this study. The DLI provide suitable results due its efficient way for structure related conduit delineation. The DLI of 1st principle component is used due to its total presentation for the lineaments of the study area. The DLI of lineament intersection of TM bands 5/7 are strongly related to the hydrothermal activities related to the Saint Catherine caldera collaplse structure.

This study demonstrates how the favorate locations for the underground water aquifer can depend on the area that has the highest watershed and the highest density of lineaments intersection. This procedure has been tested by using the Ground penetration radar tecniches for ground water detection.

### References

Amos, B. J., and D. Greenbaum, 1987. Alteration detection using TM imagery: the effects of supergene weathering in an arid environment, in Proceeding of the 21st Symposium on Remote Sensing of Environment: Environmental Research Institute of Michigan, Ann Arbor, Mich., p. 795.

Bennett, S.A., 1993. Use of thematic mapper imagery to identify mineralization in the Santa Teresa district, Sonora, Mexico, Int. Geol. Rev., 35, 1009-1029.

Beres, Milan Jr., and Haeni, F.P., 1991, Application of Ground-Penetrating-Radar Methods in Hydrogeologic Studies, Ground Water, vol.29, no.3, pp.375-386.

Collins, E. W.; Hovorka, S. D.; and Laubach, S. E., 1992, Fracture systems of the Austin Chalk, north-central Texas. In Schmoker, J. W.; Coalson, E. B.: and Brown, C.A. (Editors), Geological Studies Relevant to Horizontal Drilling: Examples from Western North America: The Rocky Mountain Association of Geologists, Denver, CO. pp. 129-142

De Marsilly, G., 1985. Flow and transport in fractured rocks: Connectivity and scale effects, in Hydrogeology of Rocks of low Permeability, Tucson, AZ., pp. 267-277.

Domenico, P. A. and Schartz, F.W., 1990, Physical and Chemical Hydrogeology: John Wiley and Sons, Inc. New York, 824 p.

El-Fouly A., (1992), Information Extraction and Integration in Mineral Exploration, University of Arizona, Tucson, Arizona.(Unpublished Ph.D. Dissertation) P.219

El-Fouly A., M.Poulton and C.Glass (1992), Hi_res: A Highly Integrated Raster Based Exploration System. IGARSS'92, International Geoscience and Remote Sensing Symposium, Vol.II, pp.935

ElFouly A., (1994). Lineament Classification, Zoning Detection, and their Applications in Mineral Exploration. The second International Confernce on Geology of the Arab World, Cairo University, Giza, Egypt.

ElFouly A., (2000). Major Structure Patterns Identification and Hydrothermal Delination using Density of Lineament Intersections. ASPRS 2000, The Image and Geospacial Information Society, Annual Convention May 23-26, 2000, Washington, DC, USA.

El-Ghawaby, M.A. and Kassem, M. (1982). Structural control of groundwater distribution in the lacustrime and alluvial deposits of Wadi Feiran, South Sinai, Egypt. Bull. Fac. Sci., Mansoura Univ. 9, 535-549.

El-Rayes, A. E. A. (1992). Hydrogeological studies of Saint Katherine area, South Sinai, Egypt. M.Sc. Thesis, Fac. Sci. Suez Canal Univ., Ismailia, 95 pp.

El-Shamy, I. Z., El-Ghawaby, M. A. and El-Rayes, A. E. A. (1989). Geologic factors affecting groundwater occurrences in the basement rocks of St. Katherine area, South Sinai, Egypt. Proc. 2nd Conf. Geol. Sinai Develop. Ismailia, 27-32.

Eriksen, A. S., and D. R. Cowan, 1989. Further development and application of GIS technology and geostatistics to assist in the exploration for uranium in western North America, in Proceedings of 7th Thematic Conference on Remote Sensing for Exploration Geology, Vol. II, Environmental Reseach Institute of Michigan, Ann Arbor, Mich., pp. 1285-1307.

Fetter, C.W., 1994, Applied Hydrogeology, Third Edition, MacMillan, New York, 691p.

Frei, M., and S. L. Jutz, 1989. Use of thematic mapper data for the detection of gold bearing formations in the eastern desert of Egypt, in Proceedings of the 7th Thematic Conference on Remote Sensing for Exploration Geology, Vol. II, Environmental Research Institute of Michigan, Ann Arbor, Mich., pp. 1157-1172.

Crippen, R. E., 1988. The dangers of underestimating the importance of data adjustments in band ratioing, Int. J. Remote Sensing, 9, 767-776.

Friedman, M. and Wiltschko, D. V., 1992, An approach to exploration for naturally fractured reservoirs, with examples from the Austin Chalk. In Schmoker, J. W.; Coalson, E. B.; and Brown, C. A. (Editors), Geological Studies Relevant to Horizontal Drilling: Examples from Western North America: The Rocky Mountain Association of Geologists Denver, Co, pp. 143-153.

Fuller, C. M. and Sharp, J. M., Jr., 1992. Premeability and fracture patterns in extrusive volcanic rocks: Implications from the welded Santana Tuff, Trans-Pecos Texas: Geological Society of America Bulletin, Vol. 104, No. 11, pp. 1485-1496.

Gale, J. E., 1982, Assessing the permeability characteristics of fractured rock. In Narasimhan, T.N. (Editor), Recent Trends in Hydrogeology: Geologic Society of America Special Paper 189, Boulder, CO, pp. 163-181.

Gale, J.E.; Rouleau, A.; and Atkinson, L.C., 1985, Hydraulic properties of fractures. In Anonymous, Hydrogeology of Rocks of Low Permeability: Tucson, AZ, pp. 1-16.

Geological survey of Egypt, 1978. Geologic map of the ?????? quadrangle, Egypt, Scale 1:250,000.

Gerlitz, K., M.D. Knoll, G.M. Cross, R.D. Luzitano, and Knight, 1993, Processing ground penetrating radar to improve resolution of near-surface targetsd, in Proc., Symposium on the Application of Geophysics to Engineering and Environmental Problems, 18-22 April 1993, San Diego, CA, 561-574.

Issar, A. and Gilad, D. (1982). Groundwater flow systems in the arid crystalline province of Southern Sinai. J. Hydrogeol. Dci. 27, No.3, 309-325.
La Pointe, P. R. and Hudson, J. A., 1985, Characterization and Interpretation of Rocks Mass Joint Patterns, Geological Society of America Special Paper 199: Geological Society of America, Boulder, CO, 37 p.

Laubach, S. E., 1992, Fracture networks in selected Cretaceous sandstones of the Green River and San Juan basins, Wyoming, New Mexico, and Colorado. In Schmoker, J. W.; Coalson, E. B.; and Brown, C. A. (Editors), Geological Studies Relevant to Horizontal Drilling: Examples from Western North America: The Rocky Mountain Association of Geologists Denver, Co, pp. 115-127.

Li, D. 1994. Fracture Water Network Analysis and Its Application to Watersupply and Underground Engineerings. In Proceedings of the Tenth Thematic Conference on Geologic Remote Sensing, vol. 2, 568-575. Ann Arbor. Ann Arbor: Environmental Research Institute of Michigan.

Long, J.C.S. and Witherspoon, P.A., 1985, The relationship of the degree of interconnection to permeability in fracture networks: Journal pf Geophysical Research, Vol. 90, No. B4, pp. 3087-3098.

Lyon, R. J. P. 1977. Mineral exploration applications of digitally processed Landsat-5 imagery. In Proceedings, first annuoal William T. Pecora memorial symposium. Government Printing Office, Washington, D.C. Geological Survey Professional Paper 1015, pp. 271-292, illus.

Mouat, D. A., J.S. Myers, and N. M. Miltron, 1986, An Integrated approach to the use of Landsat-5 TM data for gold exploration in west-central Nevada, in Proceedings of

the 5th Thematic Conference on Geologic Remote Sensing, Environmental Research Institute of Michigan, Ann Arbor, Mich., pp. 431-443.

Moorman, Brian J., Judge, Alan S., Burgess, Margo M., And Fridel, Tom W., 1994, Geotechnical Investigations of Insulated Permafrost Slopes Along The Norman Wells Pipeline Using Ground Penetrating Radar, GPR'94 Proceedings of The Fifth International Conference on Ground Penetrating Radar, vol.2, pp.477-491.

National Research Council, 1996, Rock Fractures and Fluid Flow: Comtemporary Understanding and Application: National Academy Press, Washington, DC, 551 p.

Nelson, R. A., 1985, Geologic Analysis of Naturally Fractured Reservoirs: Gulf Publishing Company, Houston, TX, 320 p.

Prost, G. L., 1988, Predicting subsurface joint trents in undeformed strata. Environmental Research Inst. Michigan, Ann Arbor: Proceedings of the Sixth Thematic Conference ob Geologic Remote Sensing, Houston, 2: 423-436.

Prost, G. L., 1996, Airphoto Fracture Analysis of the Cottonwood Creek Field, Bighorn Basin, Wyoming: SPE Prep. 35289: International Petroleum Conference and Exhibition, Villahermosa, Mexico, pp. 25-32.

Ramasamy, S., and R. Jayakumar, 1993. Behavior of the aquifer Systems in Complexity Folded and Fractured Precambrian Regimes of Southern Indian Peninsula. In Proceedings of the Ninth Thematic Conference on Geologic Remote Sensing, vol. 1, 597-607. Ann Arbor: Environmental Research Institute of Michigan.

Sharp, J.M., JR., 1993, Fractured aquifer/ reservoir: approaches, problems and opportunities: Memoirs of XXIVth Congress of the international Association of Hydrologists: AS OSLO, pp. 23-38.

Robillard, C., Nicolas, P., Armirat, P., Gariepy, M., And Goupil, F., 1994, Shallow Bedrock Profiling Using GPR, GPR '94 Proceedings of the Fifth Intrnational Conference on Ground Penetrating Radar, vol.3, pp. 1167-1179.

Rodriguez, E. P., and C. E. Glass, 1991. Digital analysis for mineral exploration at the Puerto Libertad area, Sonora, Mexico, in Proceedings of the 8th Thematic Conference on Geologic Remote Sensing, Vol. II, Environmental Research Institute of Michigan, Ann Arbor, Mich., pp. 851-862.

Shendi, E.A. (1989). New approach for locating promissing water well sites in Saint Katherine and surroundings, South Western Sinai, Egypt, M.Sc. Thesis Fac. Sci. Suez Canal Univ., Ismailia.

Schmitt, H. A., 1966, The porphyry copper deposits in their regional setting, in Titley, S.R., and Hicks, C. L., eds., Geology of the porphyry copper deposits southwestern North America: Tucson, AZ, Univ. Arizona Press, pp.17-33

Thorpe, R. K., 1980. An Example of rocks fracture Characterization for modeling purposes. In Wang, J. S. Y. and Chin, F. T., Proceedings of the Workshop on Numerical Modeling of Thermohydrologic Flow in Fractured Rocks Masses, Berkeley, CA, pp. 37-42.

Vincent, R. K., G. N. Scott, and S. Thillaigovindarajan, 1978. Groundwater Exploration in Northwestern Tamil Nadu, India with LANDSAT-5 Data. In Proceedings of the Twelfth

Symposium on Remote Sensing of Environment 2: 1053-1062. Ann Arbor: The Environmental Research Institute of Michigan.

Wilcox, R. E., Harding, T. P., and Seely, D. R., 1973, Basic wrench tectonics: American Association of Petroleum Geologists Bulletin, v. 57. 74-96.

Woodcock, N. J., and Schubert, C., 1994, Continental strike slip tectonics, in Hancock, P. L. (ed.), Continental deformation: Pergamon Press, New York, P. 251-263.